



OPEN

Biaxial strain tuned upconversion photoluminescence of monolayer WS₂

Shrawan Roy¹, Xiaodong Yang¹✉ & Jie Gao²✉

Monolayer tungsten disulfide (1L-WS₂) is a direct bandgap atomic-layered semiconductor material with strain tunable optical and optoelectronic properties among the monolayer transition metal dichalcogenides (1L-TMDs). Here, we demonstrate biaxial strain tuned upconversion photoluminescence (UPL) from exfoliated 1L-WS₂ flakes transferred on a flexible polycarbonate cruciform substrate. When the biaxial strain applied to 1L-WS₂ increases from 0 to 0.51%, it is observed that the UPL peak position is redshifted by up to 60 nm/% strain, while the UPL intensity exhibits exponential growth with the upconversion energy difference varying from – 303 to – 120 meV. The measured power dependence of UPL from 1L-WS₂ under biaxial strain reveals the one photon involved multiphonon-mediated upconversion mechanism. The demonstrated results provide new opportunities in advancing TMD-based optical upconversion devices for future flexible photonics and optoelectronics.

Keywords Upconversion photoluminescence, Biaxial strain, Monolayer WS₂

Monolayer tungsten disulfide (1L-WS₂) is a direct bandgap atomic-layered semiconductor material^{1–3}, belonging to the transition metal dichalcogenides (TMDs) family. 1L-WS₂ has been widely studied due to its promising physical properties such as high quantum yield^{4,5}, sizable spin–orbit coupling⁶, and wafer-scale uniform growth^{7,8}. Rather than the photoluminescence (PL) observed in 1L-WS₂ with the above-bandgap excitation, upconversion photoluminescence (UPL) can also be achieved in 1L-WS₂ with the below-bandgap excitation at room temperature^{9,10}. UPL represents an anti-Stokes process with the emitted photons having higher energy compared to the absorbed photons, and the phenomenon has been studied with different types of materials such as quantum wells¹¹, quantum dots¹², rare-earth-doped materials¹³, organic dyes^{14,15}, and 1L-TMDs^{9,16–18}. UPL emission has wide applications in many fields for advancing future optoelectronics such as lasers¹⁹, displays²⁰, photovoltaics²¹, bioimaging^{22,23}, and optical refrigeration²⁴.

Tunable optical and optoelectronic properties of 1L-TMDs can be achieved by using various tuning methods such as electrostatic doping²⁵, chemical treatment^{2,3,26,27}, heterostructure forming^{10,28,29}, and strain engineering^{30–32}. Among these methods, strain engineering is one effective approach to adjust the crystal lattice and band structure of 1L-TMDs, so that their optical responses are modulated such as PL emission, Raman scattering, and optical absorption^{30–36}. Strain engineering has been carried out on TMDs by multiple ways such as bending TMD layers on flexible substrates^{30,31,34–37}, forming ripples and wrinkles^{32,33,38}, and transferring TMD layers on patterned substrates^{39,40}. The study of strain engineered UPL emission from 1L-TMDs is highly demanded for realizing future tunable optical upconversion devices and flexible optoelectronic platforms. However, the strain tuned UPL emission in 1L-TMDs particularly in 1L-WS₂ has not been comprehensively investigated until now.

Here, biaxial strain tuning of UPL emission from exfoliated 1L-WS₂ at room temperature is demonstrated. By utilizing the bending and indentation method, biaxial strain is applied to the exfoliated 1L-WS₂ flakes transferred on flexible polycarbonate (PC) cruciform substrate. When the biaxial strain applied to 1L-WS₂ increases from 0 to 0.51%, the UPL peak positions are redshifted with 54 nm/% strain and 60 nm/% strain at the excitations of 685 nm and 725 nm, respectively, which are equivalent to the strain tuning gauge factors of 163 meV/% strain and 179 meV/% strain. Meanwhile, biaxial strain tuned UPL intensity in 1L-WS₂ is demonstrated to follow an exponential growth function with the upconversion energy difference in a wide range from – 303 to – 120 meV, with the enhancement of UPL intensity in nearly 75 times. The power dependence of UPL from 1L-WS₂ under biaxial strain at the excitation wavelengths of 685 nm and 725 nm elucidates the one photon involved upconversion

¹Department of Mechanical and Aerospace Engineering, Missouri University of Science and Technology, Rolla, MO 65409, USA. ²Department of Mechanical Engineering, Stony Brook University, Stony Brook, NY 11794, USA. ✉email: yangxia@mst.edu; jie.gao.5@stonybrook.edu

process assisted by multiphonon absorption. These results will offer new possibilities in facilitating TMD-based optical upconversion devices for future applications in infrared sensing, night vision, photodetection, flexible photonics and optoelectronics.

Results and discussion

The optical reflection microscope image of the mechanically exfoliated 1L-WS₂ flake transferred on flexible PC cruciform substrate is displayed in Fig. 1a. Figure 1b shows the schematic diagram of the biaxial strain apparatus with the bending and indentation method^{37,41}, where the biaxial strain is applied to 1L-WS₂ flake transferred at the center area of PC cruciform substrate pinned at its four edges by metal rods. The PC cruciform substrate is inserted between the rod assembly and the central sphere indenter. As the central sphere indenter deflects the substrate upwards, the equi-biaxial tensile strain is applied on the top surface of the substrate. The biaxial strain applied to the 1L-WS₂ flake is described by $\varepsilon = 3Dt/L^2$, where L is the distance between the two opposite pin edges ($L = 25.4$ mm), t is the thickness of the PC cruciform substrate ($t = 0.25$ mm), and D is the displacement of the central sphere indenter.

The biaxial strain tuned PL spectra excited at 532 nm and UPL spectra excited at 685 nm and 725 nm for the 1L-WS₂ sample at room temperature are presented in Fig. 2. In Fig. 2a, the PL peak position is observed at around 619 nm without strain, which matches with the typical PL spectrum of 1L-WS₂^{1–5}. The PL peak position continuously gets redshifted as the biaxial strain increases from 0 to 0.51%, with approximately 4 times

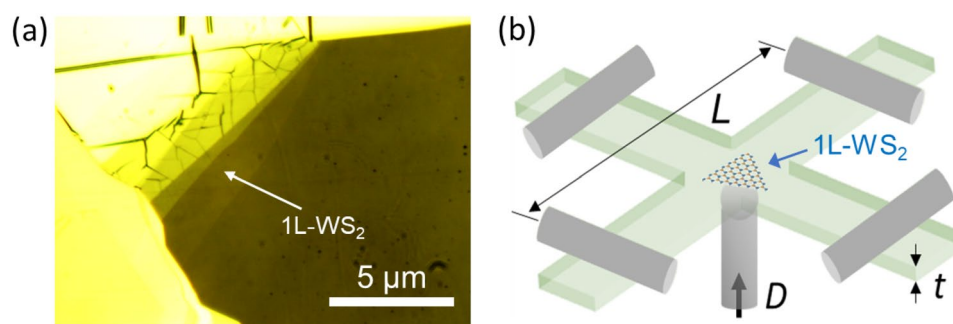


Figure 1. (a) Optical image of an exfoliated 1L-WS₂ flake transferred on flexible PC cruciform substrate. (b) Schematic diagram for the biaxial strain apparatus with the bending and indentation method.

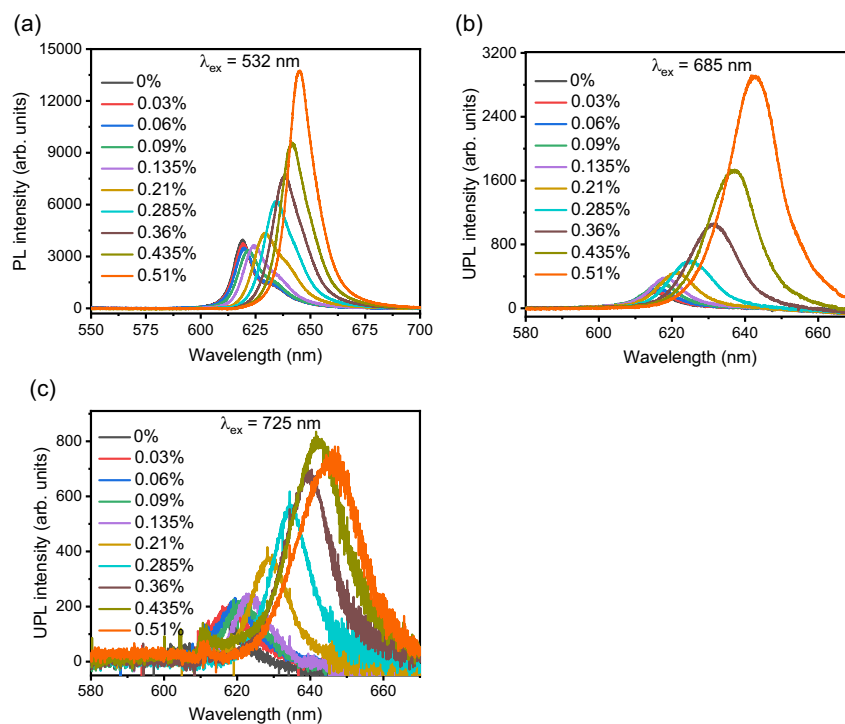


Figure 2. (a) Biaxial strain tuned PL spectra of 1L-WS₂ excited at 532 nm. (b, c) Biaxial strain tuned UPL spectra excited at 685 nm and 725 nm, respectively.

enhancement in the PL intensity. In Fig. 2b,c, the UPL peak positions without strain under the excitation wavelengths of 685 nm and 725 nm are around 616 nm, which is consistent with the PL peak position. It is observed that the UPL peak positions are also redshifted under the influence of increasing levels of applied biaxial strain, while the enhancement of UPL intensity is nearly 15 and 5 times under the excitation wavelengths of 685 nm and 725 nm, respectively. It is noted that the UPL intensity at 0.51% strain under 725 nm excitation is slightly lower compared to that at 0.435% strain, which may be resulted from the change in sample condition after several cycles of applied strain.

Figure 3a summarizes the PL and UPL peak positions as a function of the biaxial strain applied to 1L-WS₂ under different excitation wavelengths, showing a linear dependence of the peak position shift on the strain level. The PL peak position redshift of 55 nm/% strain is obtained at the excitation of 532 nm with the strain tuning gauge factor of 163 meV/% strain, which is similar to the results reported in the previous work^{37,42}. The UPL peak position redshifts at the excitations of 685 nm and 725 nm are 54 nm/% strain and 60 nm/% strain, corresponding to the strain tuning gauge factors of 163 meV/% strain and 179 meV/% strain, respectively. The slight difference between the strain tuning gauge factors at different excitation wavelengths is due to different strain transfer conditions between 1L-WS₂ and substrate during each cycle of applied strain³⁰. For the biaxial strain varied from 0 to 0.51%, the upconversion energy difference between the excitation photon energy and the UPL emission energy $\Delta E = \hbar\omega_{ex} - \hbar\omega_{UPL}$ is tuned from -205 to -120 meV at the excitation of 685 nm, and from -303 to -209 meV at the excitation of 725 nm. Figure 3b shows the dependence of the integrated UPL intensity from 1L-WS₂ on the strain tuned upconversion energy difference in the wide range of -303 to -120 meV under the excitations of 685 nm and 725 nm at room temperature. It shows that the UPL intensity follows an exponential growth function with the upconversion energy difference, with the enhancement of UPL intensity in nearly 75 times. The UPL intensity can be described by the Boltzmann function as $I_{UPL} \propto \exp(-|\Delta E|/k_B T)$, where $|\Delta E|$ is the upconversion energy gain, k_B is the Boltzmann constant, and T is the room temperature at 298 K. The effective phonon number involved in the multiphonon-assisted upconversion process in 1L-WS₂ is approximately estimated from 6 to 2, based on the ratio between $|\Delta E|$ from 303 to 120 meV and the phonon energy of 52 meV for the A_{1g} transverse optical phonon in 1L-WS₂.

The power dependent PL and UPL intensities from 1L-WS₂ excited at 532 nm, 685 nm, and 725 nm are plotted in a log-log scale in Fig. 4a,b at the biaxial strain of 0% and 0.51%, respectively. The power law of $I = \alpha P^\beta$ is used to fit the PL and UPL intensities, where P is the excitation power, α is the fitting parameter, and β is the exponent. It is observed that the β values for PL emission at both strain levels show a sublinear power dependence, which is due to the presence of nonradiative exciton-exciton annihilation at high excitation intensity. The β values for UPL emission at 0% strain also exhibit a sublinear power dependence at the excitations of 685 nm and 725 nm. At 0.51% strain, the β values increase to around 0.9, which is close to linear power dependence. The sublinear power dependence for the UPL emission may be related to the change of densities of phonons and exciton complexes⁹. The power dependence of UPL emission from 1L-WS₂ at both strain levels further indicates the one photon involved upconversion photon emission process assisted by multiphonon absorption, rather than any nonlinear optical generation of the upconversion like exciton Auger scattering or two-photon excitation-induced emission^{9,16}.

The biaxial strain dependent Raman spectra of 1L-WS₂ excited at 532 nm are presented in Fig. 5a. The Raman spectrum of 1L-WS₂ at 0% strain (black curve) clearly shows two characteristic peaks that correspond to the in-plane longitudinal optical phonon mode (E_{2g}¹) and the second-order acoustic mode [2LA(M)] at the Raman shift of ~352 cm⁻¹, and the out-of-plane transverse optical phonon mode (A_{1g}) at 419 cm⁻¹, which are consistent with the previously reported Raman modes of 1L-WS₂^{1-5,43}. It is noteworthy that the observed multiphonon-assisted UPL process is mediated by the out-of-plane A_{1g} transverse optical phonon mode, rather than the in-plane E_{2g}¹ longitudinal optical phonon mode^{9,16}. When the biaxial strain gradually increases from 0 to 0.51%, the Raman

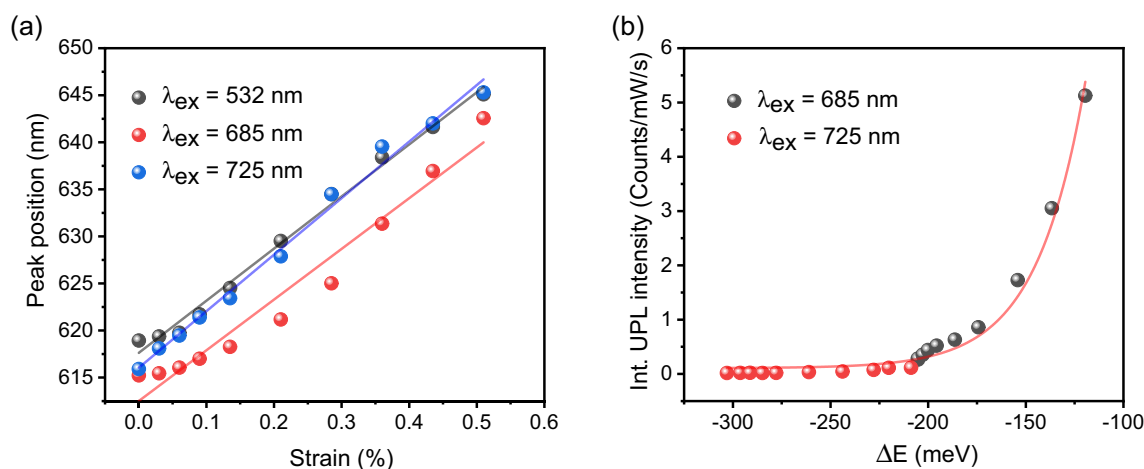


Figure 3. (a) PL and UPL peak positions as a function of the biaxial strain applied to 1L-WS₂ under different excitation wavelengths. (b) Dependence of the integrated UPL intensity on the strain tuned upconversion energy difference under the excitations of 685 nm and 725 nm.

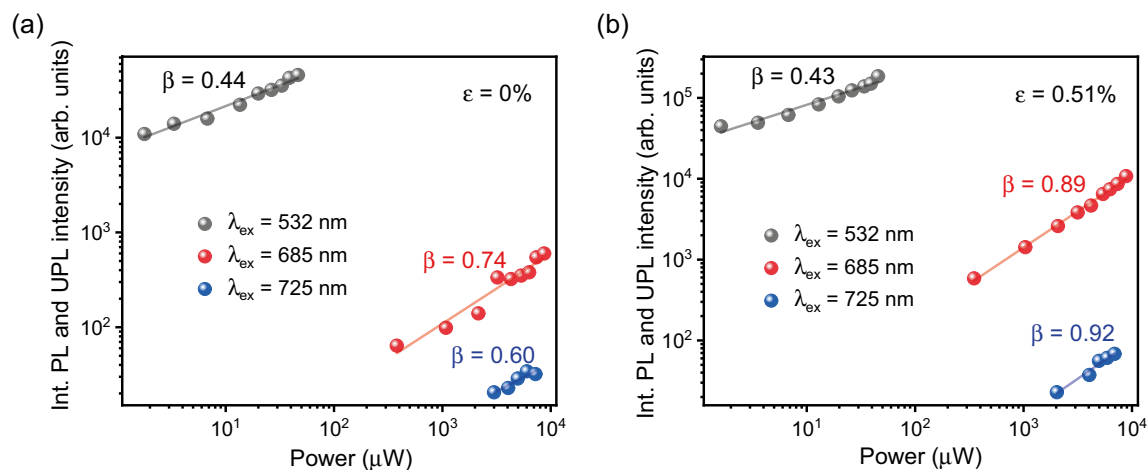


Figure 4. Power dependent integrated PL and UPL intensities in a log–log scale under the excitations of 532 nm, 685 nm, and 725 nm at the biaxial strain of (a) 0% and (b) 0.51%.

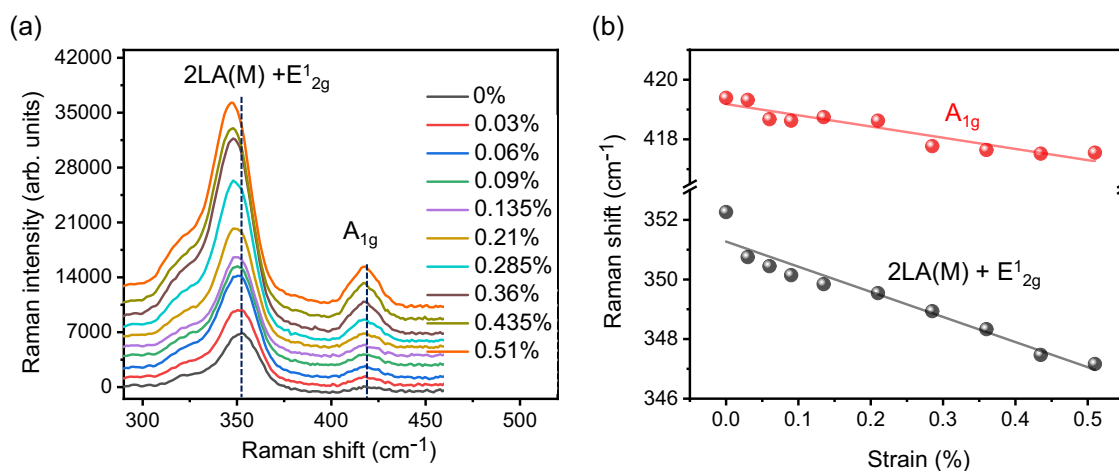


Figure 5. (a) Biaxial strain dependent Raman spectra of 1L-WS₂ excited at 532 nm. The dashed lines mark the Raman peak positions at 0% strain. (b) Raman peak positions of A_{1g} and 2LA(M) + E¹_{2g} modes depending on the biaxial strain.

peak positions of A_{1g} and 2LA(M) + E¹_{2g} vibrational modes continuously get redshifted by approximately 1.8 cm⁻¹ and 5 cm⁻¹ respectively, which is resulted from the strain induced crystal symmetry breaking and vibration softening as well as the high strain sensitivity of E¹_{2g} mode^{31,44–46}. Figure 5b plots the linear dependence of the Raman peak positions of A_{1g} and 2LA(M) + E¹_{2g} modes on the biaxial strain, showing the redshifts of 3.5 cm⁻¹/% strain and 9.99 cm⁻¹/% strain, respectively. The Raman peak position of A_{1g} mode is nearly three times less sensitive to the applied strain compared to 2LA(M) + E¹_{2g} mode, giving only slight change in the optical phonon energy around 52 meV during the strain tuned UPL emission from 1L-WS₂. It is noted that instead of its low strain sensitivity, the A_{1g} mode of 1L-WS₂ is highly sensitive to the electronic changes like electrostatic doping^{45,46}. The overall Raman intensity is increased about 3.5 times at 0.51% strain compared to that at 0% strain.

Conclusion

We have demonstrated the biaxial strain tuning of UPL emission from mechanically exfoliated 1L-WS₂ on flexible PC cruciform substrate by utilizing the bending and indentation method. The UPL peak positions get redshifted by 54 nm/% strain and 60 nm/% strain under the excitation wavelengths of 685 nm and 725 nm as the biaxial strain varies from 0% to 0.51%, which provide the strain tuning gauge factors of 163 meV/% strain and 179 meV/% strain, respectively. The strain tuned UPL intensity follows an exponential function with the upconversion energy difference in a range of – 303 to – 120 meV, with the UPL intensity enhancement of nearly 75 times. The power dependence of UPL emission from 1L-WS₂ under biaxial strain indicates the one photon involved upconversion process mediated by multiphonon absorption. The demonstrated results will enable new opportunities in promoting TMD-based tunable photon upconversion devices used for many applications such as infrared sensing, imaging, night vision, and flexible optoelectronics.

Methods

Sample preparation

1L-WS₂ flakes were mechanically exfoliated from a bulk WS₂ crystal (2D Semiconductors) with scotch tape method. Bulk WS₂ crystal was first deposited on scotch tape and exfoliated many times to obtain thin layers including monolayers, then the tape was gently placed on a small piece of polydimethylsiloxane (PDMS) film attached on glass slide for approximately 45 min. Next, the tape was gently removed to obtain multilayer and 1L-WS₂ flakes on PDMS film. 1L-WS₂ flakes were confirmed by optical microscopic image, PL, and Raman spectra. The cruciform substrate has a length of 60 mm and the width of 8 mm, which was cut from a 0.25 mm thick PC board. Finally, the exfoliated 1L-WSe₂ flakes on PDMS film were transferred to the center area of PC cruciform substrate with the dry transfer method based on an optical microscope equipped with a micromanipulator⁴⁷.

Optical measurements

PL and Raman spectra of 1L-WS₂ flakes on PC cruciform substrate were characterized with a 532 nm excitation laser by recording the back reflected signal from a 50 × objective lens (NA = 0.42) that was coupled into a spectrometer (Horiba, iHR 550) through a beam splitter and a 532 nm ultrasteep longpass edge filter. The UPL spectra were acquired by using the same measurement setup with continuous-wave excitation lasers at the wavelengths of 685 nm and 725 nm, and the corresponding 675 nm and 700 nm shortpass filters.

Data availability

The datasets generated during and/or analyzed during the current study are available from the corresponding author on reasonable request.

Received: 20 September 2023; Accepted: 9 February 2024

Published online: 15 February 2024

References

- Kim, M. S. *et al.* Biexciton emission from edges and grain boundaries of triangular WS₂ monolayers. *ACS Nano* **10**(2), 2399–2405 (2016).
- Amani, M. *et al.* Recombination kinetics and effects of superacid treatment in sulfur- and selenium-based transition metal dichalcogenides. *Nano Lett.* **16**(4), 2786–2791 (2016).
- Dhakal, K. P. *et al.* Heterogeneous modulation of exciton emission in triangular WS₂ monolayers by chemical treatment. *J. Mater. Chem. C* **5**, 6820–2827 (2017).
- Yuan, L. & Huang, L. Exciton dynamics and annihilation in WS₂ 2D semiconductors. *Nanoscale* **7**, 7402–7408 (2015).
- Roy, S. *et al.* Measurement of quantum yields of monolayer TMDs using dye-dispersed PMMA thin films. *Nanomaterials* **10**(6), 1032 (2020).
- Zhang, Y. J., Onga, M., Qin, F., Shi, W., Zak, A., Tenne, R., Smet, J. & Iwasa, Y. Optoelectronic response of a WS₂ tubular *p-n* junction. *2D Mater.* **5**, 035002 (2018).
- Wang, J. *et al.* Dual-coupling-guided epitaxial growth of wafer-scale single-crystal WS₂ monolayer on vicinal *a*-plane sapphire. *Nat. Nanotechnol.* **17**, 33–38 (2022).
- Chubarov, M. *et al.* Wafer-scale epitaxial growth of unidirectional WS₂ monolayers on sapphire. *ACS Nano* **15**(2), 2532–2541 (2021).
- Jadczak, J. *et al.* Room temperature multi-phonon upconversion photoluminescence in monolayer semiconductor WS₂. *Nat. Commun.* **10**, 107 (2019).
- Wang, Q. & Wee, T. S. Upconversion photovoltaic effect of WS₂/2D perovskite heterostructures by two-photon absorption. *ACS Nano* **15**(6), 10437–10443 (2021).
- Bacher, G. *et al.* Exciton dynamics in In_xGa_{1-x}As/GaAs quantum-well heterostructures: Competition between capture and thermal emission. *Phys. Rev. B* **47**(15), 9545 (1993).
- Deutsch, Z., Neeman, L. & Oron, D. Luminescence upconversion in colloidal double quantum dots. *Nat. Nanotechnol.* **8**(9), 649 (2013).
- Auzel, F. Upconversion and anti-Stokes processes with f and d ions in solids. *Chem. Rev.* **104**(1), 139 (2004).
- Zhao, J., Ji, S. & Guo, H. Triplet-triplet annihilation based upconversion: from triplet sensitizers and triplet acceptors to upconversion quantum yields. *RSC Adv.* **1**(6), 937 (2011).
- Baluschev, S. *et al.* Up-conversion fluorescence: noncoherent excitation by sunlight. *Phys. Rev. Lett.* **97**(14), 143903 (2006).
- Jones, A. M. *et al.* Excitonic luminescence upconversion in a two-dimensional semiconductor. *Nat. Phys.* **12**, 323 (2016).
- Manca, M. *et al.* Enabling valley selective exciton scattering in monolayer WSe₂ through upconversion. *Nat. Commun.* **8**, 14927 (2017).
- Mushtaq, A., Yang, X. & Gao. Unveiling room temperature upconversion photoluminescence in monolayer WSe₂. *Opt. Express* **30**, 45212–45220 (2022).
- He, G. S., Markowicz, P. P., Lin, T.-C. & Prasad, P. N. Observation of stimulated emission by direct three-photon excitation. *Nature* **415**(6873), 767–770 (2002).
- Downing, E., Hesselink, L., Ralston, J. & Macfarlane, R. A three-color, solid-state, three-dimensional display. *Science* **273**(5279), 1185–1189 (1996).
- Gray, V., Dzebo, D., Abrahamsson, M., Albinsson, B. & Moth-Poulsen, K. Triplet-triplet annihilation photon-upconversion: towards solar energy applications. *Phys. Chem. Chem. Phys.* **16**(22), 10345–10352 (2014).
- Vinegoni, C., Razansky, D., Hilderbrand, S. A., Shao, F., Ntziachristos, V. & R. Weissleder, Transillumination fluorescence imaging in mice using biocompatible upconverting nanoparticles. *Opt. Lett.* **34**(17), 2566–2568 (2009).
- Xu, C. T. *et al.* Autofluorescence insensitive imaging using upconverting nanocrystals in scattering media. *Appl. Phys. Lett.* **93**(17), 171103 (2008).
- Epstein, R. I., Buchwald, M. I., Edwards, B. C., Gosnell, T. R. & Mungan, C. E. Observation of laser-induced fluorescent cooling of a solid. *Nature* **377**(6549), 500–503 (1995).
- Plechinger, G. *et al.* Identification of excitons, trions and biexcitons in single-layer WS₂. *Phys. Status Solidi RRL* **9**, 457–461 (2015).
- Roy, S. *et al.* Atomic observation of filling vacancies in monolayer transition metal sulfides by chemically sourced sulfur atoms. *Nano Lett.* **18**(7), 4523–4530 (2018).
- Peimyo, N. *et al.* Chemically driven tunable light emission of charged and neutral excitons in monolayer WS₂. *ACS Nano* **8**, 11320–11329 (2014).

28. Roy, S. *et al.* Modulation of optoelectric properties of monolayer transition metal dichalcogenides placed on a metal pattern. *J. Korean Phys. Soc.* **78**, 693–699 (2021).
29. Gong, Y. *et al.* Vertical and in-plane heterostructures from WS₂/MoS₂ monolayers. *Nat. Mater.* **13**, 1135–1142 (2014).
30. Carrascoso, F., Li, H., Frisenda, R. & Castellanos-Gomez, A. Strain engineering in single-, bi- and tri-layer MoS₂, MoSe₂, WS₂ and WSe₂. *Nano Res.* **14**(6), 1698–1703 (2021).
31. Wang, F., Li, S., Bissett, M. A., Kinloch, I. A., Li, Z. & Young, R. J. Strain engineering in monolayer WS₂ and WS₂ nanocomposites. *2D Mater.* **7**, 045022 (2020).
32. Lee, J. *et al.* Switchable, tunable, and directable exciton funneling in periodically wrinkled WS₂. *Nano Lett.* **21**(1), 43–50 (2021).
33. Dhakal, K. P. *et al.* Local strain induced band gap modulation and photoluminescence enhancement of multilayer transition metal dichalcogenides. *Chem. Mater.* **29**(12), 5124–5133 (2017).
34. Island, J. O. *et al.* Precise and reversible band gap tuning in single-layer MoSe₂ by uniaxial strain. *Nanoscale* **8**, 2589–2593 (2016).
35. Desai, S. B. *et al.* Strain-induced indirect to direct bandgap transition in multilayer WSe₂. *Nano Lett.* **14**(8), 4592–4597 (2014).
36. Wu, W. *et al.* Giant mechano-optoelectronic effect in an atomically thin semiconductor. *Nano Lett.* **18**(4), 2351–2357 (2018).
37. Carrascoso, F., Frisenda, R. & Castellanos-Gomez, A. Biaxial versus uniaxial tuning of single layer MoS₂. *Nano Mater. Sci.* **4**(1), 44–51 (2022).
38. Wang, J. *et al.* Strain epitaxy of monolayer transition metal dichalcogenides for wrinkle arrays. *ACS Nano* **15**(4), 6633–6644 (2021).
39. Chaste, J. *et al.* Intrinsic properties of suspended MoS₂ on SiO₂/Si pillar arrays for nanomechanics and optics. *ACS Nano* **12**(4), 3235–3242 (2018).
40. Li, H. *et al.* Optoelectronic crystal artificial atoms in strain-textured molybdenum didulphide. *Nat. Commun.* **6**, 7381 (2015).
41. Androulidakis, C. *et al.* Graphene flakes under controlled biaxial deformation. *Sci. Rep.* **5**, 18219 (2016).
42. Aslan, B., Deng, M. & Heinz, T. F. Strained bilayer WSe₂ with reduced exciton-phonon coupling. *Phys. Rev. B* **98**, 115308 (2018).
43. Wang, X. H., Zheng, C. C. & Ning, J. Q. Influence of curvature strain and Van der Waals force on the inter-layer vibration mode of WS₂ nanotubes: A confocal micro-Raman spectroscopic study. *Sci. Rep.* **6**, 33091 (2016).
44. Li, Z., *et al.* Efficient strain modulation of 2D materials via polymer encapsulation. *Nat Commun.* **11**, 1151 (2020).
45. Kim, M. S. *et al.* Enhanced light emission from monolayer semiconductors by forming heterostructures with ZnO thin films. *ACS Appl. Mater. Interfaces* **8**(42), 28809–28815 (2016).
46. Roy, S. *et al.* Observation of charge transfer in heterostructures composed of MoSe₂ quantum dots and a monolayer of MoS₂, or WSe₂. *J. Phys. Chem. C* **121**(3), 1997–2001 (2017).
47. Zhao, Q., Wang, T., Ryu, Y. K., Frisenda, R. & Castellanos-Gomez, A. J. An inexpensive system for the deterministic transfer of 2D materials. *Phys. Mater.* **3**, 016001 (2020).

Acknowledgements

The authors acknowledge the support from the DARPA (W911NF2110353).

Author contributions

J.G., X.Y. and S.R. conceived the idea of the research. S.R. performed the experiments. J.G. and X.Y. directed the research. All authors discussed the results and contributed to the manuscript.

Competing interests

The authors declare no competing interests.

Additional information

Correspondence and requests for materials should be addressed to X.Y. or J.G.

Reprints and permissions information is available at www.nature.com/reprints.

Publisher's note Springer Nature remains neutral with regard to jurisdictional claims in published maps and institutional affiliations.



Open Access This article is licensed under a Creative Commons Attribution 4.0 International License, which permits use, sharing, adaptation, distribution and reproduction in any medium or format, as long as you give appropriate credit to the original author(s) and the source, provide a link to the Creative Commons licence, and indicate if changes were made. The images or other third party material in this article are included in the article's Creative Commons licence, unless indicated otherwise in a credit line to the material. If material is not included in the article's Creative Commons licence and your intended use is not permitted by statutory regulation or exceeds the permitted use, you will need to obtain permission directly from the copyright holder. To view a copy of this licence, visit <http://creativecommons.org/licenses/by/4.0/>.

© The Author(s) 2024